Geophysical Research Letters

RESEARCH LETTER
10.1029/2020GL088206

What Caused the Large-Scale Heat Deficit in the Subtropical South Atlantic Ocean During 2009–2012?

Shenfu Dong[1], Hosmay Lopez[1], Sang-Ki Lee[1], Christopher S. Meinen[1], Gustavo Goni[1], and Molly Baringer[1]

[1]NOAA/Atlantic Oceanographic and Meteorological Laboratory, Miami, FL, USA

Key Points:
- The subtropical South Atlantic Ocean showed a large heat deficit during the 2009–2012 period
- This heat deficit is largely driven by oceanic heat transport divergence, especially the reduced Ekman transport across 35°S
- The reduced Ekman transport is remotely forced in part by cooling in the central tropical Pacific

Supporting Information:
- Supporting Information S1

Correspondence to:
S. Dong,
shenfu.dong@noaa.gov

Citation:
Dong, S., Lopez, H., Lee, S.-K., Meinen, C. S., Goni, G., & Baringer, M.. (2020). What caused the large-scale heat deficit in the subtropical South Atlantic Ocean during 2009–2012?. *Geophysical Research Letters*, *47*, e2020GL088206. https://doi.org/10.1029/2020GL088206

Received 31 MAR 2020
Accepted 24 APR 2020
Accepted article online 29 APR 2020

Abstract The subtropical South Atlantic hosts complex ocean circulation patterns and processes that transport heat to the North Atlantic, thereby playing an important role in global energy redistribution. This study uses several oceanic products to assess ocean heat changes in the subtropical South Atlantic and the associated atmosphere-ocean processes. A particular focus is placed on the large heat deficit during 2009–2012, which is associated with cooling during 2008–2011 and subsequent warming. This heat deficit was largely driven by a sharp increase in the southward Ekman transport across 35°S during 2008–2011. The anomalous Ekman transport is connected to the persistent positive sea level pressure anomaly over the Atlantic sector of the Southern Ocean, caused by the Southern Annular Mode and the Pacific-South American Modes. Although the overall correlations of these climate modes with the Ekman transport are modest during 1993–2016, the modes combined to produce large heat content anomalies during 2009–2012.

Plain Language Summary Recent studies have shown that changes in ocean heat content in the South Atlantic can have a pronounced impact on regional and global extreme weather events and long-term climate variability. Motivated by these findings, this study addresses the physical mechanisms responsible for a large heat content deficit during 2009–2012, which is associated with cooling during 2008–2011 and subsequent warming during 2012–2013. Observation-based examination of the two main forcing mechanisms for ocean heat content changes, air-sea heat exchange, and ocean heat convergence indicates that the observed heat deficit is largely driven by oceanic heat transport divergence, especially the direct wind-forced southward transport anomalies across 35°S. This anomalous southward transport is consistent with positive sea level pressure (SLP) anomalies south of 37°S and negative SLP anomalies to the north during this period. This spatial pattern of the SLP anomalies resembles the SLP spatial structure forced by cooling in the central Pacific.

1. Introduction

More than 90% of the excess heat gained by Earth system over the past 50 years has been absorbed by the ocean (Levitus et al., 2012; Rhein et al., 2013; Trenberth et al., 2014), which has motivated numerous studies to understand ocean heat content (OHC) changes on various spatial and temporal scales (e.g., Häkkinen et al., 2013; Roemmich et al., 2015; Desbruyères et al., 2017, 2016; Zanna et al., 2019). An accurate estimate and diagnosis of regional OHC changes is crucial not only for closing the global energy budget, but also for monitoring and understanding changes in climate and weather patterns.

The main sources of regional OHC changes are air-sea heat exchange and the advective heat divergence by oceanic currents, including both Ekman and geostrophic currents. The relative contributions of these two terms (i.e.,air-sea heat exchange and advective heat divergence) in altering OHC vary both in space and time. The ocean heat budget in the subtropical South Atlantic has not been studied with observations in as much detail as other basins due to limitations in available data. The sparsity of in situ data has also resulted in underestimation of ocean warming in the South Atlantic (Durack et al., 2014; Durack & Wijffels, 2010). However, changes in the South Atlantic Ocean have been shown to impact regional and global precipitation patterns, surface air temperature, and the shift of the Intertropical Convergence Zone (Haarsma et al., 2003; Nnamchi & Li, 2011; Nobre et al., 2012; Bombardi et al., 2014; Lopez, Dong, Lee, & Goni, 2016; Xue, Li, et al., 2018, Xue, Sun, et al., 2018). The objective of this study is to examine the recently observed OHC changes in the subtropical South Atlantic and to investigate what caused this observed variability, with a particular focus on a large heat deficit that occurred during 2009–2012.

2. Data Sets and Methodology

Several data sets (Table S1 in the supporting information) are used in this study to examine OHC changes in the subtropical South Atlantic. The World Ocean Database (WOD) provides OHC estimates for the upper 700 m from 1955 to the present, and for the upper 2,000 m from 2005 to the present; both products are provided on a 1° × 1° grid and at 3-month temporal resolutions (Levitus et al., 2012). Monthly temperature and salinity products are available from the following: the Simple Ocean Data Assimilation version 3.4.2 (SODA3, Carton et al., 2018); the Met Office Hadley Center objective analysis version 4.2.1 (EN4, Good et al., 2013); and the gridded fields of Argo data from the Scripps Institution of Oceanography (SIO, Roemmich & Gilson, 2009). The SODA3 data set is available from 1980 to 2017 on a 0.5 × 0.5° grid with 50 vertical levels; the vertical layer thickness increases from ~10 m near the surface to ~200 m below 2,000 m depth. The EN4 data set is available from 1900 to the present on a 1° × 1° grid with 42 vertical levels—the vertical layer thickness increases from 10 m near the surface to 300 m below 3,000 m depth. The gridded Argo data from SIO are available for upper 2,000 m from 2004 to the present on a 1° × 1° grid with 58 vertical levels.

In addition to the gridded/assimilated OHC estimates from hydrography, monthly satellite altimetry sea surface height (SSH) data produced by Ssalto/Duacs and distributed by Aviso (Ducet et al., 2000) are used to derive a heat content proxy, where SSH is regressed to OHC from SODA3 at each grid point for the 2005–2016 period. This time period is chosen because of the consistency in OHC variations among different products as will be discussed in the following section. SODA3 is chosen only based on its temporal and spatial resolution, which match those of the altimeter gridded product better because the regression is done on each grid point. Results are very similar when other OHC estimates (WOD, EN4 or Argo) are used in the regression, indicating good consistency among different estimates for the chosen period. This OHC proxy from SSH is estimated throughout the continuous altimetry period from 1993 to 2016.

Air-sea heat fluxes (surface turbulent and radiative fluxes, positive into the ocean) from the ERA-Interim product suite (Dee et al., 2011) are also used in analyzing the heat budget; these data are available on a 0.75° × 0.75° grid with monthly resolution since 1979. Monthly meridional heat transport at 20°S and 35° S is estimated by using a combination of satellite and in situ measurements following the methods used in Dong et al. (2015). A short description of the methodology is given in the supporting information (Text S1). Note that unlike in Dong et al. (2015), to be consistent with the air-sea heat fluxes and other data used in this study, the Ekman transport contributions to meridional heat transport are estimated using wind stress from ERA-Interim instead of the NCEP reanalysis winds used in that earlier study. The monthly mean 850 hPa geopotential height, sea level pressure (SLP), and sea surface temperature (SST) from ERA-Interim are also used in this study to explore the impact of the large-scale atmospheric circulation on the OHC changes in the South Atlantic Ocean.

This study focuses on OHC variations on interannual and longer time scales. Therefore, a monthly climatology was removed from each variable and a 13-month running average was applied to exclude signals with shorter periods. Note that estimates of degrees of freedom for the significance of error bars for trends in OHC and correlations between oceanic heat transport and climate indices were determined based on a decorrelation time scale of 1 year.

3. Variations in the Subtropical South Atlantic Ocean Heat Content

To obtain an initial estimate of the dominant scales of the OHC variations at interannual time periods, an empirical orthogonal function (EOF) analysis was performed on the detrended SSH and OHC data in the South Atlantic (10–40°S, 65°W to 25°E). The leading mode of SSH shows a dipole pattern with anomalies of opposite sign north and south of 20°S (Figure1a). The time evolution of this dipole mode is dominated by oscillations with periods of 4–6years (Figure1b). The spatial patterns of the leading modes of each of the OHC data sets are noisier (FigureS1 in the supporting information). Therefore, instead of showing the results from EOF analysis, Figures1c–1e show the regression patterns of the detrended OHC to the leading SSH mode for SODA3, EN4, and WOD, respectively. Although somewhat noisy, all three regressions show dipole patterns similar to the leading EOF mode of SSH. This dipole pattern resembles the dominant mode of SST variability in the region, the South Atlantic subtropical dipole, which is thought to be driven by the

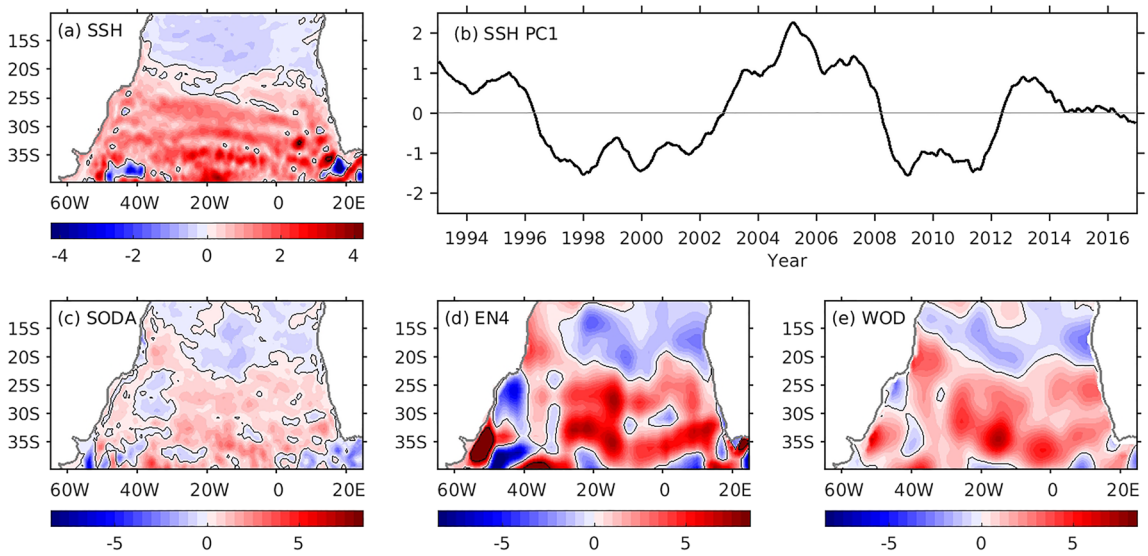

FIGURE 1. (a) Spatial pattern and (b) time series of the leading empirical orthogonal function (EOF) of detrended monthly sea surface height (SSH) in the Subtropical South Atlantic during 1993–2016. (c)–(e) Regression pattern of ocean heat content to the time series of SSH leading EOF for SODA, EN4, and WOD, respectively.

variability of the westerlies and southeasterlies (e.g., Haarsma et al., 2005; Morioka et al., 2011; Nnamchi et al., 2011; Rodrigues et al., 2015).

Figure 2a shows the interannual variations of anomalous OHC averaged in the region between 20°S and 35° S. OHC changes averaged over a larger region (10–35°S) are very similar, but slightly weaker due to compensation in the region between 10°S and 20°S (Figure S2 in the supporting information). The smaller region was chosen because of the readily available meridional heat transport estimates at 20°S and 35°S, which can be used to investigate their contributions to OHC change. In addition, the variability of the subtropical dipole (Figure 1) is dominated by the southern lobe, which is covered largely by the chosen region (20°S to 35°S). Although the OHC estimates from all four products show significant increase from 1993 to 2016, the rates of increase are quite different. OHC from EN4 exhibits the highest rate of increase with $7.4 \pm 1.4 \times 10^{21}$ Joules per decade (trend ±95% error bar based on Student's *t* test), while that from WOD (upper 700 m) shows the lowest rate of increase with $2.6 \pm 1.4 \times 10^{21}$ Joules per decade. The OHC trends from the SODA3 and SSH proxy data sets are in between, $3.6 \pm 1.4 \times 10^{21}$ and $5.2 \pm 1.1 \times 10^{21}$ Joules per decade, respectively. We note that SIO gridded Argo data are only available beginning in 2004, therefore the OHC trend during the entire 24-year period (1993–2016) cannot be determined with Argo data. Differences are also seen between the results from the various products when evaluating the interannual variations, particularly for the pre-Argo period before 2005. OHC from SODA3 experiences slightly higher frequency changes than those from other products. Beginning in 2005, all data sets agree very well in both the interannual variations and the trends. All OHC estimates show a consistent decrease from 2008 to 2011 and an increase afterward, resulting in a large heat deficit during 2009–2012. Note that, as indicated by the WOD heat content in the upper 700 m and 2,000 m, most of the variations are in the upper 700 m. This is also the case for SODA3 and EN4 data (Figure S3 in the supporting information).

Given that all these data products are derived from more or less the same historical hydrographic observations (Table S1 in the supporting information), differences in the OHC estimates are mainly due to the objective mapping methods and quality control procedures being applied. The better agreement in OHC changes beginning in 2005 among different data sets is likely attributable to the arrival of the Argo float measurements, which largely improved the spatial and temporal coverage of observations in the data-limited South Atlantic. The improved data coverage would reduce the sensitivity of the OHC estimates to mapping methods. The impact of the Argo availability on those data sets can also be seen in a comparison of the time rates of change of the OHC (heat storage rates) (Figure 2b). Before 2005, the heat storage rates do not agree among different data sets, whereas beginning in 2005 the heat storage rates are more consistent among the

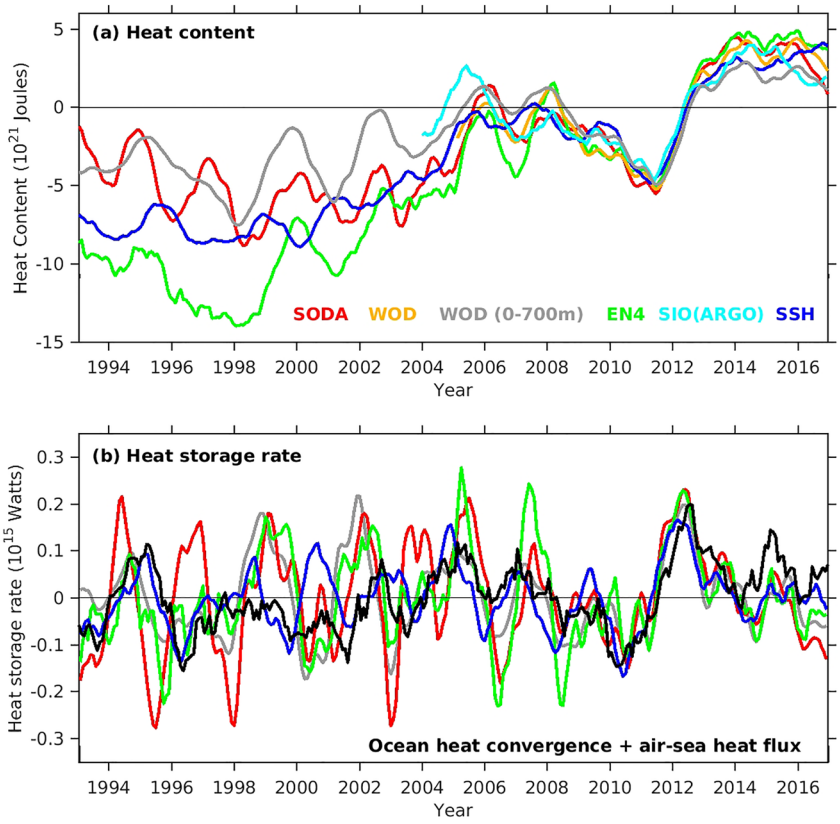

FIGURE 2. (a) Interannual variations of the ocean heat content (OHC) in the South Atlantic averaged between 20°S and 35°S for upper 2,000 m water column from WOD (gold), SODA3 (red), EN4 (green), SIO gridded Argo data (cyan), and SSH proxy (blue), and for upper 700 m from WOD (gray). (b) Heat storage rate corresponding to the heat content data in (a) and the sum of the ocean heat convergence and air-sea heat fluxes (black), the two main contributors to the ocean heat content changes.

data sets. Also included in Figure 2b is the sum of surface air-sea heat fluxes and ocean heat convergence ($MHT_{35°S}$–$MHT_{20°S}$), which agree well with the heat storage rate beginning in 2005. The correlations with all four heat storage rate estimates exceed the 95% significance level of 0.40, varying from $r = 0.54$ (EN4) to $r = 0.74$ (SSH proxy). Before 2005, only the heat storage rate derived from SSH significantly correlates with the sum of the air-sea heat fluxes and the ocean heat convergence ($r = 0.56$).

4. What Caused the Subtropical South Atlantic Ocean Heat Content Changes?

Changes in OHC can result from variations in air-sea heat exchange and/or from ocean heat convergence. To examine the contributions of these two sources to the strong cooling/warming periods during 2008–2011/2012–2013, we compute the time integral of the surface flux and ocean heat convergence for the period of 2005–2016 (Figure 3a). It is very clear that the cooling during 2008–2011 is largely due to the anomalous oceanic heat convergence. Surface heat fluxes play a secondary role in the cooling after 2010, but act to damp the cooling before 2010. Not surprisingly, the rate of heat content change is not completely balanced by the sum of air-sea heat fluxes and oceanic heat convergence, due to errors in the data and uncertainties in the gridded products. We further divide the ocean heat convergence into the geostrophic and Ekman components (Figure 3b). The results clearly demonstrate the dominance of the Ekman transport component, which contributes about 77% of the total ocean heat convergence-based cooling from 2008 to mid-2011. Examination of the Ekman transports across 20°S and 35°S (Figure 3d) indicates that the Ekman transport across 35°S plays a dominant role, particularly after 2009. About 68% of the total ocean heat convergence-based cooling from Ekman transports comes from the southward transport anomalies across 35°S. The contribution of the Ekman transport across 20°S to this cooling event mainly occurs during the first two years

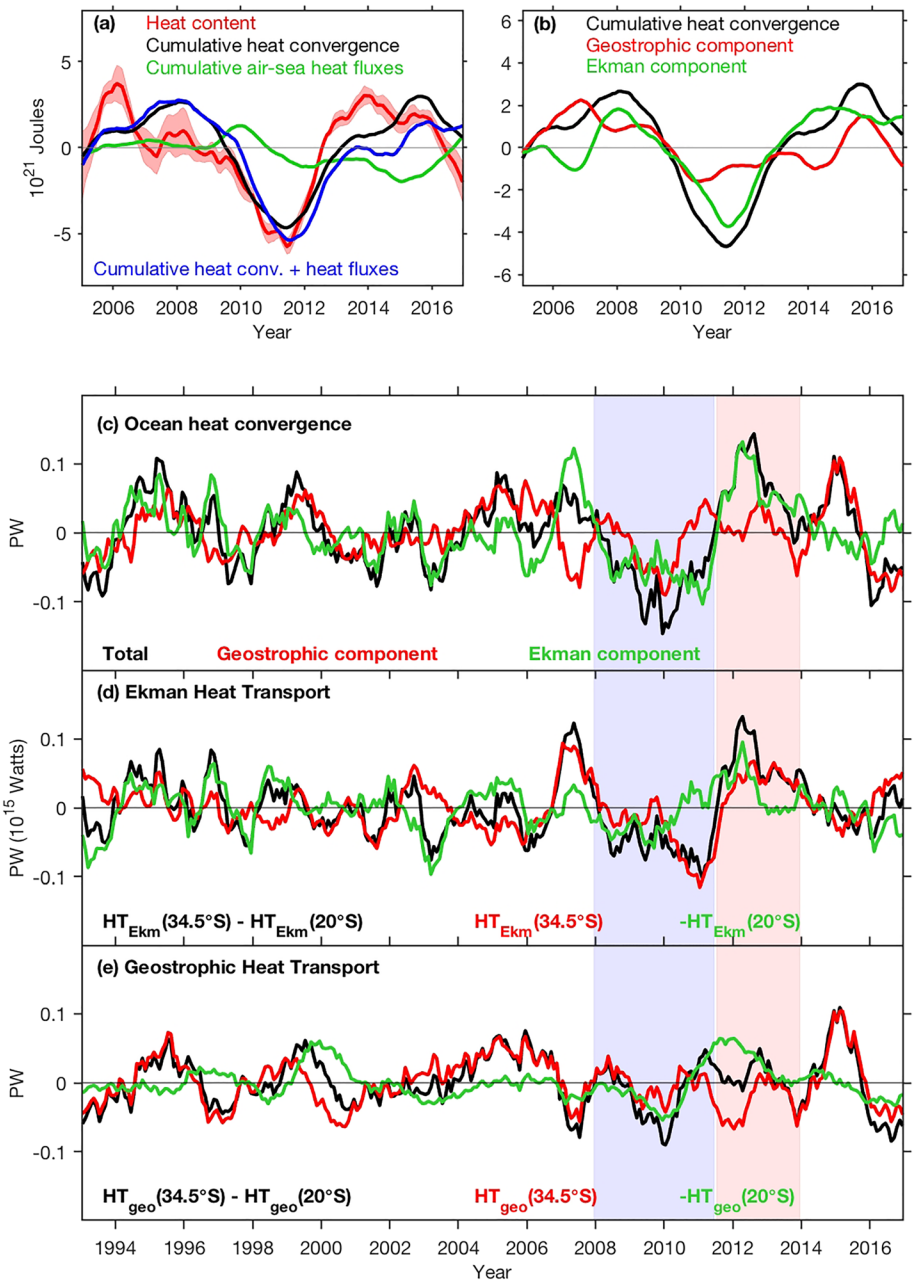

FIGURE 3. (a) Ocean heat content from SODA3 (red) and time integrals of the ocean heat convergence (black), surface air-sea heat flux (green), and their sum (blue). The shading for OHC denotes two standard deviation of different products. (b) Time integrals of the ocean heat convergence (black) and its geostrophic (red) and Ekman (green) components. (c) Time series of ocean heat convergence in the region between 20°S and 35°S (black) and contributions from the geostrophic (red) and Ekman (green) transport. (d) Ocean heat convergence from the Ekman transport (black) and Ekman heat transport at 20°S (green) and 35°S (red). (e) Similar to (b) but for geostrophic transport component. Units are in petawatts (PW).

(2008–2009). By contrast, the weaker cooling associated with the geostrophic transports (Figure 3e) is dominated by the anomalous northward transport across 20°S (68%), with the southward geostrophic transport anomalies at 35°S playing a secondary role.

The Ekman transports acquired an even more dominant role in the subsequent warming during 2012–2013, explaining 98% of the ocean heat convergence-based warming. Similar to the cooling period, the northward

Ekman transport anomalies across 35°S during mid-2011 to 2013 account for 64% of the total warming effects from oceanic transport. The remaining 36% that results from the southward Ekman transport anomalies across 20°S is concentrated during the first half the warming period. The minimal role of the geostrophic transports in the warming is due to compensation of the transport anomalies across 20°S and 35°S.

When the entire 24-year period is considered, the geostrophic and Ekman transports play nearly equal roles in the total oceanic heat convergence, with the geostrophic transports playing a slightly larger role, explaining 54% of the total variance of the oceanic heat convergence (Figures 3c–3e). The roughly equal distribution of variance at the two boundaries is also the case for the Ekman flows when considering the entire time record, with the Ekman transports across 20°S and 35°S both contributing about half of the total variance in the Ekman convergence. As shown in Figure 3d, the Ekman transport across 20°S dominates the variations in the Ekman transport convergence during 1993–2006, whereas after 2006 the Ekman transport across 35°S dominates. In terms of the geostrophic process, the geostrophic heat convergence is largely controlled by the transport across 35°S, except during the 2008–2013 event (Figure 3e).

In summary, our analysis indicates that, over a longer time period, both geostrophic and Ekman transports play equal roles in OHC variations in the subtropical South Atlantic. The dominance of the geostrophic and Ekman transports varies with time. The anomalous large heat deficit during 2009–2012, induced by the 2008–2011 cooling and subsequent warming during 2012–2013, was largely forced by the anomalous Ekman transport across 35°S. Because of the importance of OHC in the climate system, and the possibility of reoccurrence of such event in the future, understanding what caused this anomalous event will be beneficial.

5. Impact of the Large-Scale Atmospheric Circulation on South Atlantic Heat Content

Changes in the South Atlantic on interannual time scales have been linked to the leading modes of the atmospheric variability in the Southern Hemisphere: the Southern Annular Mode (SAM), and the Pacific-South American mode 2 (PSA2) (e.g., Mo & Higgins, 1998; Mo & Paegle, 2001; Rodrigues et al., 2015). The SAM is commonly defined as the leading empirical orthogonal function (EOF) of Southern Hemisphere 850 hPa geopotential height, while the second and third EOFs are used to define the Pacific-South American (PSA) patterns, PSA1 and PSA2, respectively. Variations in the PSA patterns are known to be linked to tropical heating anomalies in the central Pacific, which generate wave trains extending poleward and eastward to the South Atlantic (e.g., Mo & Higgins, 1998; Rodrigues et al., 2015). In this study, EOF analysis was performed on the area-weighted monthly mean 850 hPa geopotential height south of 15°S to define these indices (Figure S4 in the supporting information). These indices were then used to examine the forcing mechanisms for the anomalous Ekman transport across 35°S, the largest contributor to the heat deficit in the South Atlantic during 2009–2012 as shown in Figure 3.

The spatial patterns of SLP corresponding to SAM, PSA1, and PSA2 (Figures 4b–4d), were derived by regressing SLP onto the SAM, PSA1, and PSA2 indices (Figure 4a), respectively. The positive phase of the SAM is characterized by a strengthening and poleward shift of the westerly wind belt, normally centered around 55°S (Figure 4b), resulting in stronger westerlies in the region 50–70°S and weaker westerlies in the midlatitudes (30–50°S). The reduced westerlies (i.e., easterly anomalies) in the midlatitudes during positive SAM should induce southward Ekman transport anomalies. Therefore, we expect a negative correspondence between SAM and Ekman transport across 35°S, which is consistent with the opposite anomalies in the SAM and Ekman heat transport at 35°S shown in Figure 4a. During the 24-year period, the correlation of the Ekman transport at 35°S with SAM is $r = -0.41$, barely exceeding the 95% significance level of $r = 0.40$. The high-latitude South Atlantic Ocean exhibits low-pressure anomalies during the positive phase of PSA2 (Figure 4d). As a result, the midlatitude South Atlantic Ocean experiences westerly anomalies during positive PSA2 events and consequently exhibits anomalous northward Ekman transports. This is consistent with the positive correlation between the Ekman transport at 35°S and PSA2 shown in Figure 4a, although the correlation coefficient of $r = 0.34$ is only marginally significant at the 90% level. During the positive phase of PSA1, the subtropical South Atlantic is featured with low-pressure anomalies centered at 35°S (Figure 4c), which results in minimal wind changes at this latitude. This explains the low correlation of the Ekman transport with PSA1 ($r = 0.10$). During the time period of 2001–2013, the correspondences

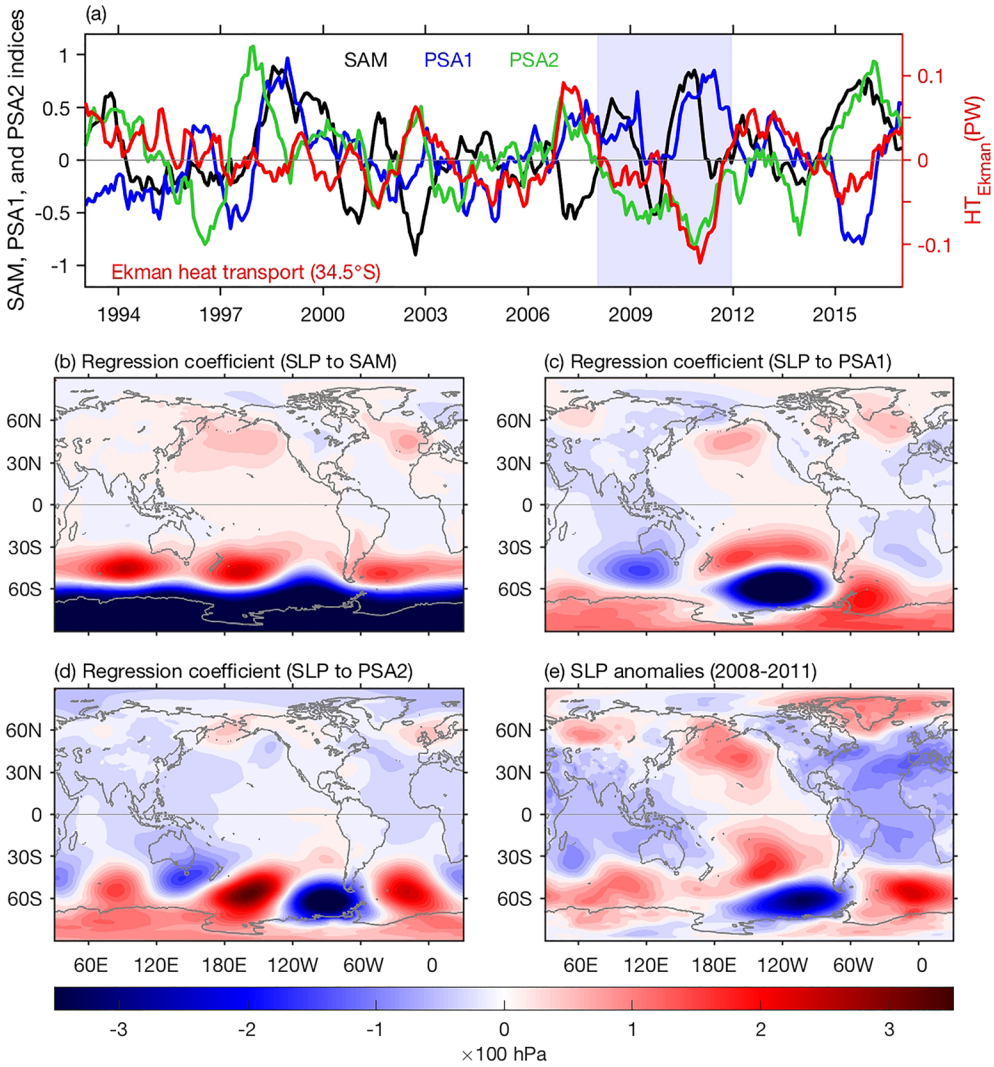

FIGURE 4. (a) Time series of the Ekman heat transport at 35°S (red, right axis) and indices of the SAM (black), PSA1 (blue), and PSA2 (green). (b)–(d) Spatial distributions of the sea level pressure corresponds to SAM, PSA1, and PSA2, respectively. Note that the sign for PSA2 pattern is reversed, the distribution corresponds to the negative phase of PSA2. (e) The anomalous sea level pressure during the cooling period 2008–2011.

between the Ekman transport and both SAM and PSA2 are much better, with correlation coefficients of $r = -0.58$ and 0.63, respectively. The SAM and PSA2 are out of phase during this time period, thus working together to force the anomalous southward Ekman transport at 35°S and therefore the negative heat content anomaly in the South Atlantic. However, during other periods, the two indices tend to be in phase and work against each other in terms of forcing the Ekman transport anomalies, which could partially account for the low correlations of Ekman transport with SAM and PSA2 for the entire 24-year period. Although the Ekman heat transport at 35°S also controls the subsequent warming during 2012–2013, there is no simple relationship with the SAM or PSA2 indices.

The SLP anomalies averaged during the 2008–2011 cooling period are shown in Figure 4e. The spatial structure of these 4-year averaged SLP anomalies well resembles the PSA2 pattern (Figure 4e) with reversed sign, particularly in the South Atlantic Ocean. The resemblance of the SLP spatial patterns in Figures 4d and 4e in the South Atlantic Ocean (0–60°S, 60°W to 20°E) is indicated by their correlation of $r = -0.83$. Although to a lesser degree, the positive anomalies in SLP between 35°S and 50°S and negative anomalies north of 37°S in the South Atlantic are also consistent with the SAM SLP pattern (Figure 4b). Although the resemblance of

PSA1 pattern to the SLP anomalies in the South Atlantic Ocean is low, it contributes slightly to the negative SLP north of 35°S. The positive SLP anomalies south of 35°S and the negative anomalies to the north would result in anomalous easterlies, which in turn would induce southward Ekman transport anomalies, consistent with the observed negative (southward) Ekman heat transport during this time period. This suggests that the 2008–2011 cooling event can be explained by changes in PSA2 and SAM, with PSA2 playing a larger role. This conclusion stresses that the South Atlantic OHC is affected by the remote influence of the tropical Pacific, as suggested by Lopez, Dong, Lee, and Campos (2016). Consistent with the lack of relationship between the 2012–2013 warming and the SAM or PSA2 indices, the SLP anomalies during this warming period (not shown) do not resemble the PSA2 pattern nor the SAM pattern.

As discussed earlier, the PSA2 has been linked to the central Pacific SST anomalies. The positive phase of PSA2 is associated with warming in the central Pacific, as illustrated by the spatial pattern of SST derived by regressing SST onto the PSA2 index (Figure S5d in the supporting information). The equatorial Pacific was mostly dominated by strong La Niña conditions during 2008–2011, with cooling in the central Pacific except the El Niño condition during 2009/2010 (Figures S5a and S6 in the supporting information). Although the negative phase of PSA2 is consistent with the La Niña conditions, the observed cooling in the subtropical South Atlantic is opposite to the expected warming in the region during the negative phase of PSA2 (e.g., Rodrigues et al., 2015). A possible explanation is that the previous findings were mainly focused on seasonal SST evolution, and the warming was linked to the reduced heat loss to the atmosphere due to the weakened westerlies, whereas this 4-year cooling event is dominated by the oceanic processes, that is, the southward Ekman transport anomalies associated with the weakened westerlies. This is consistent with the argument that the air-sea heat fluxes play a large role for SST and upper ocean heat content changes on seasonal to short time scales, whereas on interannual to longer time scales oceanic processes dominate (Buckley et al., 2015; Dong et al., 2007; Dong & Kelly, 2004; Vivier et al., 2002).

6. Conclusions

Recent studies have shown that changes in the South Atlantic Ocean (SST, OHC) can have a pronounced impact on regional and global extreme weather events and long-term climate variability. Motivated by these findings, our study addressed the physical mechanisms responsible for the large OHC deficit during 2009–2012, which is a dominant feature of the OHC in the subtropical South Atlantic during the recent observational period. It was found that the largest contributor to both the 2008–2011 cooling that leads to the 2009–2012 deficit, and to the subsequent 2012–2013 warming, is anomalous Ekman heat transports across 35°S. The southward Ekman transport anomalies during 2008–2011 are consistent with the positive SLP anomalies south of 37°S and negative SLP anomalies to the north during this period. The spatial pattern of the SLP anomalies during the cooling period resembles the SLP spatial structure for negative phase of PSA2, demonstrating a remote influence from the central Pacific. The southward shift of the westerlies associated with a positive phase of SAM during this period also favors anomalous southward Ekman transport. Therefore, SAM and PSA2 worked constructively to produce large OHC anomalies in the subtropical South Atlantic during 2008–2011. However, the correlations of those climate modes with the Ekman transports in the South Atlantic are modest during 1993–2016.

Although the Ekman process dominated the specific event during the 2008–2013 period, both the geostrophic and Ekman transports play similar-sized roles in the total ocean heat convergence during the broader 24-year study period (1993–2016), with geostrophic transport playing a slightly larger role. The dominance of the geostrophic and Ekman transports on OHC changes in the subtropical South Atlantic varies during different time periods, suggesting that the forcing mechanisms for OHC changes in the region are complex.

This study, along with others, has aided in advancing our understanding of the oceanic processes controlling OHC in the South Atlantic. However, further investigations of the complex ocean circulations in this region have been hampered by the scarcity of available observations compared to other ocean basins, particularly for the pre-Argo period. Argo floats have greatly improved ocean sampling in regions deeper than the 2,000 m isobath; however, an improved sampling in the shallower water regions is needed to produce better heat content estimates. Given the fact that prior research has shown that changes in the South Atlantic OHC could modulate decadal variability of global monsoon rainfall via interhemispheric Hadley circulation

(Lopez, Dong, Lee, & Goni, 2016), the results presented here show the value of further research in this area. In particular, a series of climate modeling experiments, where the observed large-scale 2009–2012 heat deficit in the South Atlantic Ocean is prescribed, are planned to assess its potential impact on global monsoons and extreme weather events.

Acknowledgments
The authors appreciate the comments of several anonymous reviewers which helped improve an earlier version of this manuscript. The ocean heat content from World Ocean Database is available at this site (https://www.nodc.noaa.gov/OC5/3M_HEAT_CONTENT/). The temperature and salinity fields were downloaded from http://www.atmos.umd.edu/~ocean/index_files/ for SODA3.4.2, from https://www.metoffice.gov.uk/hadobs/en4/index.html for EN4, and from http://www.argo.ucsd.edu/Gridded_fields.html for SIO gridded Argo data. The satellite altimetry SSH data are available at this site (https://www.aviso.altimetry.fr/en/data/data-access.html). The ERA-Interim products were downloaded from this site (https://www.ecmwf.int/en/forecasts/datasets/reanalysis-datasets/era-interim). This work was supported by NOAA's Climate Observation Division and the Physical Oceanography Division of NOAA-AOML. H. L. was supported in part under the auspices of the Cooperative Institute for Marine and Atmospheric Studies (CIMAS), a cooperative institute of the University of Miami and NOAA, cooperative agreement NA10OAR4320143.

References

Bombardi, R. J., Carvaldo, L. M., Jones, C., & Reboita, M. S. (2014). Precipitation over eastern South America and the South Atlantic sea surface temperature during neutral ENSO periods. *Climate Dynamics*, *42*(5–6), 1553–1568. https://doi.org/10.1007/s00382-013-1832-7

Buckley, M. W., Ponte, R. M., Forget, G., & Heimbach, P. (2015). Determining the origins of advective heat transport convergence variability in the North Atlantic. *Journal of Climate*, *28*(10), 3943–3956. https://doi.org/10.1175/JCLI-D-14-00579.1

Carton, J. A., Chepurin, G. A., & Chen, L. (2018). SODA3: A new ocean climate reanalysis. *Journal of Climate*, *31*, 6967–6983. https://doi.org/10.1175/JCLI-D-18-0149.1

Dee, D. P., Uppala, S. M., Simmons, A. J., Berrisford, P., Poli, P., Kobayashi, S., et al. (2011). The ERA-Interim reanalysis: Configuration and performance of the data assimilation system. *Quarterly Journal of the Royal Meteorological Society*, *137*(656), 553–597. https://doi.org/10.1002/qj.828

Desbruyères, D., McDonagh, E. L., King, B. A., & Thierry, V. (2017). Global and full-depth ocean temperature trends during the early twenty-first century from Argo and repeat hydrography. *Journal of Climate*, *30*(6), 1985–1997. https://doi.org/10.1175/JCLI-D-16-0396.1

Desbruyères, D. G., Purkey, S. G., McDonagh, E. L., Johnson, G. C., & King, B. A. (2016). Deep and abyssal ocean warming from 35 years of repeat hydrography. *Geophysical Research Letters*, *43*, 10,356–10,365. https://doi.org/10.1002/2016GL070413

Dong, S., Goni, G., & Bringas, F. (2015). Temporal variability of the Meridional Overturning Circulation in the South Atlantic between 20°S and 35°S. *Geophysical Research Letters*, *42*, 7655–7662. https://doi.org/10.1002/2015GL065603

Dong, S., Hautala, S. L., & Kelly, K. A. (2007). Interannual variations in upper-ocean heat content and heat transport convergence in the western North Atlantic. *Journal of Physical Oceanography*, *37*(11), 2682–2697. https://doi.org/10.1175/2007JPO3645.1

Dong, S., & Kelly, K. A. (2004). Heat budget in the Gulf Stream region: The importance of heat storage and advection. *Journal of Physical Oceanography*, *34*(5), 1214–1231. https://doi.org/10.1175/1520-0485(2004)034<1214:HBITGS>2.0.CO;2

Ducet, N., Le Traon, P.-Y., & Reverdin, G. (2000). Global high resolution mapping of ocean circulation from TOPEX/POSEIDON and ERS-1 and -2. *Journal of Geophysical Research*, *105*(C8), 19,477–19,498. https://doi.org/10.1029/2000JC900063

Durack, P. J., Gleckler, P., Landerer, F., & Taylor, K. E. (2014). Quantifying underestimates of long-term upper-ocean warming. *Nature Climate Change*, *4*(11), 999–1005. https://doi.org/10.1038/nclimate2389

Durack, P. J., & Wijffels, S. E. (2010). Fifty-year trends in global ocean salinities and their relationship to broad-scale warming. *Journal of Climate*, *23*, 4342–4362. https://doi.org/10.1175/2010JCLI3377.1

Good, S. A., Martin, M. J., & Rayner, N. A. (2013). EN4: Quality controlled ocean temperature and salinity profiles and monthly objective analyses with uncertainty estimates. *Journal of Geophysical Research: Oceans*, *118*, 6704–6716. https://doi.org/10.1002/2013JC009067

Haarsma, R. J., Campos, E., & Molteni, F. (2003). Atmospheric response to South Atlantic SST dipole. *Geophysical Research Letters*, *30*, 1864. https://doi.org/10.1029/2003GL017829

Haarsma, R. J., Campos, E. J. D., Hazeleger, W., Severijns, C., Piola, A. R., & Molteni, F. (2005). Dominant modes of variability in the South Atlantic: A study with a hierarchy of ocean-atmosphere models. *Journal of Climate*, *18*(11), 1719–1735. https://doi.org/10.1175/JCLI3370.1

Häkkinen, S., Rhines, P. B., & Worthen, D. L. (2013). Northern North Atlantic sea surface height and ocean heat content variability. *Journal of Geophysical Research*, *118*, 3670–3678. https://doi.org/10.1002/jgrc.20268

Levitus, S., Antonov, J. I., Boyer, T. P., Baranova, O. K., Garcia, H. E., Locarnini, R. A., et al. (2012). World ocean heat content and thermosteric sea level change (0–2000 m), 1955–2010. *Geophysical Research Letters*, *39*, L10603. https://doi.org/10.1029/2012GL051106

Lopez, H., Dong, S., Lee, S. K., & Campos, E. (2016). Remote influence of Interdecadal Pacific oscillation on the South Atlantic meridional overturning circulation variability. *Geophysical Research Letters*, *43*(15), 8250–8258. https://doi.org/10.1002/2016GL069067

Lopez, H., Dong, S., Lee, S. K., & Goni, G. (2016). Decadal modulations of interhemispheric global atmospheric circulations and monsoons by the South Atlantic meridional overturning circulation. *Journal of Climate*, *29*, 1831–1851. https://doi.org/10.1175/JCLI-D-15-0491.1

Mo, K. C., & Higgins, R. W. (1998). The Pacific–South American modes and tropical convection during the southern hemisphere winter. *Monthly Weather Review*, *126*(6), 1581–1596. https://doi.org/10.1175/1520-0493(1998)126<1581:TPSAMA>2.0.CO;2

Mo, K. C., & Paegle, J. N. (2001). The Pacific-South American modes and their downstream effects. *International Journal of Climatology.*, *21*(10), 1211–1229. https://doi.org/10.1002/joc.685

Morioka, Y., Tozuka, T., & Yamagata, T. (2011). On the growth and decay of the subtropical dipole mode in the South Atlantic. *Journal of Climate*, *24*(21), 5538–5554. https://doi.org/10.1175/2011JCLI4010.1

Nnamchi, H. C., & Li, J. (2011). Influence of the South Atlantic Ocean dipole on West African summer precipitation. *Journal of Climate*, *24*(4), 1184–1197. https://doi.org/10.1175/2010JCLI3668.1

Nnamchi, H. C., Li, J., & Anyadike, R. N. C. (2011). Does a dipole mode really exist in the South Atlantic Ocean? *Journal of Geophysical Research*, *116*, D15104. https://doi.org/10.1029/2010JD015579

Nobre, P., De Almeida, R. A., Malagutti, M., & Giarolla, E. (2012). Coupled ocean–atmosphere variations over the South Atlantic Ocean. *Journal of Climate*, *25*(18), 6349–6358. https://doi.org/10.1175/JCLI-D-11-00444.1

Rhein, M., Rintoul, S. R., Aoki, S., Campos, E., Chambers, D., Feely, R. A., et al. (2013). Observations: Oceans. In T. Stocker, et al. (Eds.), *Climate Change 2013*: The physical science basis. Contribution of working group I to the fifth assessment report of the intergovernmental panel on climate change, (pp.255–316). Cambridge, U.K., and New York: Cambridge Univ. press. https://doi.org/10.1017/CBO9781107415324.01

Rodrigues, R. R., Campos, E. J. D., & Haarsma, R. J. (2015). The impact of ENSO on the South Atlantic subtropical dipole mode. *Journal Climate*, *28*(7), 2691–2705. https://doi.org/10.1175/JCLI-D-14-00483.1

Roemmich, D., Church, J., Gilson, J., Monselesan, D., Sutton, P., & Wijffels, S. (2015). Unabated planetary warming and its ocean structure since 2006. *Nature Climate Change*, *5*(3), 240–245. https://doi.org/10.1038/nclimate2513

Roemmich, D., & Gilson, J. (2009). The 2004–2008 mean and annual cycle of temperature, salinity, and steric height in the global ocean from the Argo Program. *Progress in Oceanography*, *82*(2), 81–100. https://doi.org/10.1016/j.pocean.2009.03.004

Trenberth, K. E., Fasullo, J. T., & Balmaseda, M. A. (2014). Earth's energy imbalance. *Journal of Climate*, *27*(9), 3129–3144. https://doi.org/10.1175/JCLI-D-13-00294.1

Vivier, F., Kelly, K. A., & Thompson, L. (2002). Heat budget of the Kuroshio extension region: 1993–99. *Journal of Physical Oceanography*, *32*(12), 3436–3454. https://doi.org/10.1175/1520-0485(2002)032<3436:HBITKE>2.0.CO;2

Xue, J., Li, J., Sun, C., Zhao, S., Mao, J., Dong, D., et al. (2018). Decadal-scale teleconnection between South Atlantic SST and Southeast Australia surface air temperature in austral summer. *Climate Dynamics*, *50*(7–8), 2687–2703. https://doi.org/10.1007/s00382-017-3764-0

Xue, J., Sun, C., Li, J., & Mao, J. (2018). South Atlantic forced multidecadal teleconnection to the midlatitude South India Ocean. *Geophysical Research Letters*, *45*, 8480–8489. https://doi.org/10.1029/2018GL078990

Zanna, L., Khatiwala, S., Gregory, J. M., Ison, J., & Heimbach, P. (2019). Global reconstruction of historical ocean heat storage and transport. *Proceedings of the National Academy of Sciences*, *116*(4), 1126–1131. https://doi.org/10.1073/pnas.1808838115